Hindawi
Complexity
Volume 2019, Article ID 5358316, 9 pages
https://doi.org/10.1155/2019/5358316

Research Article

Tracking Control for Hydrogen Fuel Cell Systems in Zero-Emission Ferry Ships

Mohammad Hassan Khooban,[1] **Navid Vafamand**,[2] **and Jalil Boudjadar**[1]

[1]*Department of Engineering, Aarhus University, Åbogade 34, 8200 Aarhus N, Denmark*
[2]*Department of Power and Control, Shiraz University, Shiraz 71946-84471, Iran*

Correspondence should be addressed to Mohammad Hassan Khooban; mhkhoban@gmail.com

Received 11 June 2019; Revised 10 August 2019; Accepted 23 September 2019; Published 15 November 2019

Guest Editor: Taesic Kim

For more than a century, conventional marine vessels spatter the atmosphere with CO_2 emissions and detrimental particles when operated by diesel motors/generators. Fuel cells have recently emerged as one of the most promising emission-free technologies for the electrification of ship propulsion systems. In fuel cell-based ship electrification, the entire marine power system is viewed as a direct current (DC) microgrid (MG) with constant power loads (CPLs). A challenge of such settings is how to stabilize the voltages and currents of the ship's grid. In this paper, we propose a new modified backstepping controller to stabilize the MG voltage and currents. Finally, to study the performance and efficiency of our proposal, we run an experiment simulation using dSPACE real-time emulator.

1. Introduction

Nowadays, air emissions (e.g., carbon dioxide (CO_2) and sulfur dioxide gases) are changing habitats all over the world. Big parts of these air emissions originate from burning distinct forms of fuel in cars, vessels, and aircraft. According to the International Maritime Organization (IMO), the massive marine transport system streaming through oceans and seas accounts for 2% of the global world CO_2 emission. Nevertheless, vessels play a significant role in the international trading system, providing occupations and transportation as well as supporting offshore businesses like fishing [1–4].

Even though marine vessel emissions have not been considered in the Kyoto accord, stringent rules have been established by first world countries. For instance, the European Union (EU) has applied stringent rules to control and monitor the sulfur dioxide emission in exclusively sensitive sea zones, containing the Baltic Sea Zones and the Western European seas. In the mentioned zones, the fuel utilized in marine vessel systems should not contain sulfur over 0.1%. But, in most ship fuels, this value is more than 1%. Thus, the importance of developing substitutive renewable energy supplies has become a significant problem for the marine vessel propulsion [5, 6].

One of the most promising renewable energy source technologies, which can be utilized in marine power systems, is fuel cell (FC) systems [7]. FCs, dissimilar to energy storage devices, utilize an outside supply of the hydrogen and oxygen to generate power and work as long as the hydrogen gas and oxygen source are sustained [8, 9]. The main advantages of FCs, which cause them as the best possible alternative marine power source, are their great power production density, efficiency, reliability, and durability [1]. In general, a hydrogen fuel cell converts oxygen and hydrogen (or air) into the direct current power. In practice, fuel cells in most immobile and mobile vehicle applications are paired with other power electronic devices (such as DC/DC boost converters) to improve the performance and reliability of the whole system and also accurately regulate the output voltage of the FC [10]. There have been very few successful implementations of FCs for vehicles [7] and marine applications [9, 11, 12] in the past few years. Most of the existing results for the FCs use linearized representation and controllers [13]. To improve the performance, nonlinear control methods such as model predictive [14], intelligent-based PID [15], and sliding mode control [10, 16] are presented. However, in a marine power system with FC, power electronic devices and loads can be considered as a kind of mobile DC microgrid with constant

power loads (CPLs). In other words, FC in the special DC maritime MG is considered as a distributed generation, and ship motors and loads can be considered as CPLs, whenever a load is regulated to keep constant output power. Now, by considering this particular case study, a robust and high-performance controller is required to stabilize the voltage and current of the marine power grid, which is not investigated in the abovementioned approaches.

Up to now, many different approaches are suggested to reduce the detrimental effects of CPLs in DC maritime MGs [17–25]. Passive damping and active damping are two elementary methods to solve this issue [17]. In passive damping resistors, by increasing damping resistors to the filters, the destructive effect of CPLs can be mitigated. In spite of the fact that this technique has some advantages (e.g., it is simple and effective), it generates a huge dissipation [10]. On the other hand, active damping applies a modified control loop, which operates a virtual resistor [18]. In general, in active damping methods, the power is actively injected into the grid to diminish the effects of CPLs [19]. Furthermore, the methods based on small-signal models for the active damping can only guarantee system stability close to the operating point. In [17, 26], the model predictive controller is proposed for controlling the switching function of a converter that it sources a constant power load. Nevertheless, according to its computational burden, the proposed control method is not useful for real-time high-order industrial applications [27]. In [28], by controlling the duty ratio, a new modified nonlinear controller based on the sliding mode technique is suggested to stabilize a buck converter that it sources a constant power load. The proposed method in [14] can easily stabilize the whole system under any operating range changes. Nonetheless, this approach needs to measure the current of the capacitor, which is very expensive and causes ripple filtering degradation and the output impedance increase [29]. However, in those approaches, it is assumed that the DC source is ideal and the source current is independent of its voltage. This assumption is not applicable to the marine systems fed by FCs.

To sum up, this work studies an adaptive tracking control for hydrogen fuel cell systems in maritime applications. The marine power system with fuel cell and power electronic devices can be regarded as a special mobile stand-alone DC microgrid with constant power loads. Therefore, we first investigate a dynamic model of a special DC MG with CPLs for the marine power system by considering fuel cell and ship motors. Next, we extract the mathematical model of the whole system to apply the proposed control technique. Then, we develop a backstepping nonlinear control approach to stabilize the voltage and current of the ship's grid. From the control engineering viewpoint, the main difficulty in utilizing a backstepping controller for the fuel cell-based marine power systems is that the overall structure of the fuel cell does not belong to the strict-feedback form and the virtual control inputs are not affine. Therefore, in this paper, we propose a novel control method to achieve the tracking issue of the DC MG voltage and currents. The proposed control is inspired by conventional backstepping controller methods. Finally, we apply the dSPACE real-time emulator system to investigate the performance and effectiveness of our approach for marine applications.

2. Stand-Alone DC Marine Microgrid Dynamics

In general, a marine power system with a fuel cell (as a main source of the ship power), power electronic devices (as interfaces for renewable energy systems), and loads (like ship motors and navigation systems) can be considered as a special mobile islanded DC microgrid with constant power loads. Figure 1 presents the general concept of maritime DC MG with CPLs.

In the maritime systems, for the case of a ship constant speed, the ship engine should generate a constant torque. Therefore, it should receive constant power. However, in practice, any voltage fluctuations may change the power of the ship engine. Here, in this paper, the concept of the CPL is utilized in which the ship engine consuming power is tightly regulated by a DC/DC converter, and the DC bus voltage variation will not affect the ship speed. Besides the ship engine, which is assumed to act as a CPL behavior, resistive loads of the ship are also connected by the DC bus. Consequently, the fuel cell generator must feed a CPL and resistive loads. It is proved that the nonlinear CPLs degrade the stability of the DC MG, and if the voltage and/or the current of the DC bus vary from the equilibrium operating point of the system, then the overall DC MG will be unstable, which leads to a sudden drop in the DC bus voltage and spoils the CPL behavior. On the other hand, the fuel cell is a slow-response generator and any small perturbation on the DC MG makes it unstable. This fact shows the necessity of the active control of the DC bus voltage and the fuel cell power, as well, to assure the closed-loop stability and performance. To theoretically assure the stability, it is necessary to derive the state-space representation of the maritime DC MG.

Now, we work on extracting the mathematical model of the islanded marine DC MG with CPLs extracted. Totally, in the special case study of this paper, the fuel cell is used as a main power source of the ship to reduce the cost of fossil fuels and air emissions. Moreover, the power electronic devices (e.g., DC/DC boost converter) are utilized to connect the fuel cell, ship engine, and load to the DC bus link. Figure 2 shows the circuit diagram of the stand-alone DC marine MG with the fuel cell and a CPL. In this work, the ship engine is considered as a constant power load to tightly regulate the speed of the marine vessel system via a DC/DC converter. The mathematical model of the case study based on Figure 2 can be written as follows [10, 30]:

$$\frac{dV_{CPL}}{dt} = \frac{1}{C_b}\left(i_{hfc}\left(1-u_1\right) - \frac{P_{CPL}}{V_{CPL}} - \frac{V_{CPL}}{R}\right), \tag{1}$$

$$\begin{aligned}\frac{di_{hfc}}{dt} = &-\frac{nR_{ohm}}{L}i_{hfc} - \frac{n}{L}V_{at} - \frac{V_{CPL}}{L}\left(1-u_1\right)\\ &+ \frac{nR_gT_{st}}{2LF_{ar}}\left(\ln\left(P_{H_2}\right) + \frac{1}{2}\ln\left(P_{O_2}\right)\right)\\ &+ \frac{n}{2LF_{ar}}\left(\Delta G_1 + \Delta s_1\left(T_{st} - T_{hfc}\right)\right),\end{aligned} \tag{2}$$

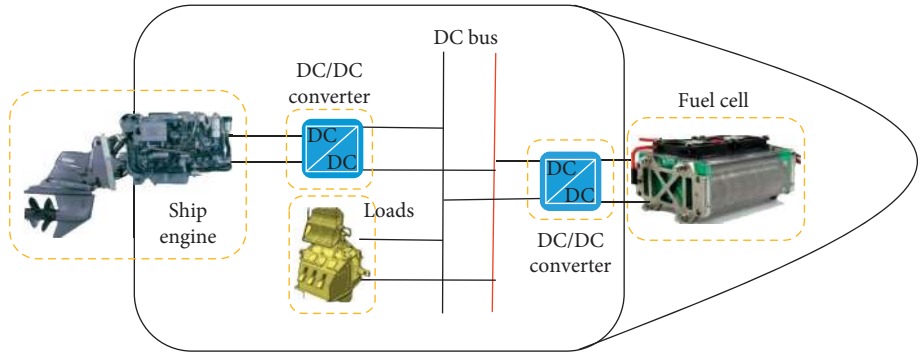

Figure 1: The overall scheme of the stand-alone DC zero-emission ferry ships.

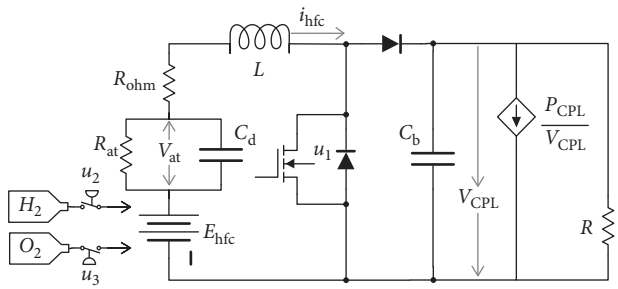

Figure 2: Circuit diagram of the marine DC MG with a fuel cell and a CPL.

$$\frac{dV_{at}}{dt} = \frac{i_{hfc}}{C_d} - \frac{V_{at}}{R_{at}C_d}, \tag{3}$$

$$\frac{dP_{H_2}}{dt} = -\frac{P_{H_2}}{\tau_{H_2}} + \frac{q_{H_2}^{in} - 2k_\gamma i_{hfc}}{\tau_{H_2}k_{H_2}}, \tag{4}$$

$$\frac{dP_{O_2}}{dt} = -\frac{P_{O_2}}{\tau_{O_2}} + \frac{q_{O_2}^{in} - 2k_\gamma i_{hfc}}{\tau_{O_2}k_{O_2}}, \tag{5}$$

$$\frac{dq_{H_2}^{in}}{dt} = \frac{u_2 - q_{H_2}^{in}}{\tau_{qH_2}}, \tag{6}$$

$$\frac{dq_{O_2}^{in}}{dt} = \frac{u_3 - q_{O_2}^{in}}{\tau_{qO_2}}. \tag{7}$$

As shown in Figure 2, a proton exchange membrane fuel cell has been applied in this study to transform the chemical energy liberated during the electrochemical reaction of hydrogen and oxygen to electrical energy [31].

The detailed definition and value of the system parameters can be found in [10]. Also, the nominal values of the parameters of the system are provided in Table 1. The control inputs u_1, u_2, and u_3 are related to the DC/DC converter connected to the fuel cell and the injecting hydrogen and oxygen flows of the fuel cell. These control inputs will be designed by applying the backstepping control as explained in Section 3.

Table 1: The parameters of the DC marine microgrid.

Parameter and definition	Nominal value
F_{ar} (Faraday constant)	96485.309 C/mol
T_{st} (fuel cell operating temperature)	353 K
T_{hfc} (fuel cell reference temperature)	298.15 K
R_g (universal gas constant)	8.3143 J/(mol.K)
ΔG (Gibbs free energy)	237160.89 J/mol
ΔS (standard molar entropy)	164.025 J/(mol.K)
τ_{H_2} (hydrogen actuator flow rate valve time constant)	3.37 sec
τ_{O_2} (oxygen actuator flow rate valve time constant)	6.47 sec
K_γ (consumed hydrogen flow rate)	9.07×10^{-8} mol/C
K_{H_2} (hydrogen molar constant)	4.22×10^{-5} Kmol.atm/sec
K_{O_2} (oxygen molar constant)	2.11×10^{-5} Kmol.atm/sec
n (number of fuel cells)	5
C_d (double-layered capacitor)	35×10^{-6} F
R_{ohm} (variable internal resistor of the fuel cell)	1.5 Ω
L_{DC} (DC/DC converter inductor)	4×10^{-3} H
C_{DC} (DC/DC converter inductor)	5×10^{-4} F
P_{CPL} (CPL power)	400 W
R (ship resistive load)	80 Ω

3. Modified Backstepping Controller

In this section, we present the procedure of designing the backstepping controller. Since the two desired references are introduced, the backstepping design procedure is split into two parts. The primary control objective is to manipulate the DC/DC boost converter that stabilizes the voltage of the DC bus V_{CPL} toward its desired value V_{ref}. The control signal is then used to generate pulse-width modulation (PWM) gate signals for the converter [32]. Moreover, the secondary goal is to manipulate the fuel cell generator to provide the power to the loads. Assuming that the DC/DC converter is ideal and does not consume power, therefore, the generated power should be equal to the demand power. Here, since only CPLs are considered, the total power demand will be the net sum of the instantaneous CPL power. Without loss of generality, consider one CPL with the power level P_{CPL} and the one resistive load R. Thus, the current should track the reference [32] $I_{ref} = P_{totall}/V_{thfc}$, where $P_{totall} = P_{cpl} + (V_{CPL}^2/R)$ and V_{thfc} is the voltage of the fuel cell and input of the DC/DC converter, computed as follows [10]:

$$
\begin{aligned}
V_{\text{thfc}} &= nV_{\text{hfc}},\\
V_{\text{hfc}} &= E_{\text{hfc}} - i_{\text{hfc}}R_{\text{ohm}} - V_{\text{at}},\\
E_{\text{hfc}} &= \frac{1}{2F_{\text{ar}}}\Big(\Delta G_1 + \Delta s_1\left(T_{\text{st}} - T_{\text{hfc}}\right)\\
&\quad + R_{\text{g}}T_{\text{st}}\Big(\ln\left(P_{\text{H}_2}\right) + \frac{1}{2}\ln\left(P_{\text{O}_2}\right)\Big)\Big).
\end{aligned}
\tag{8}
$$

For the dynamic (1), the goal of V_{CPL} is tracking V_{ref}. Defining the error $e_1 = V_{\text{CPL}} - V_{\text{ref}}$ and variable change $v_1 = 1 - u_1$ results in

$$
\dot{e}_1 = \dot{V}_{\text{CPL}} - \dot{V}_{\text{ref}} = -\frac{P_{\text{CPL}}}{C_{\text{b}}V_{\text{CPL}}} - \frac{V_{\text{CPL}}}{C_{\text{b}}R} - \dot{V}_{\text{ref}} + \frac{i_{\text{hfc}}}{C_{\text{b}}}v_1. \tag{9}
$$

Let us choose the control input v_1 as

$$
v_1 = \frac{C_{\text{b}}}{i_{\text{hfc}}}\left(-\gamma_1 e_1 + \frac{P_{\text{CPL}}}{V_{\text{CPL}}C_{\text{b}}} + \frac{V_{\text{CPL}}}{C_{\text{b}}R} + \dot{V}_{\text{ref}}\right), \tag{10}
$$

the dynamic (9) will be then

$$
\dot{e}_1 = -\gamma_1 e. \tag{11}
$$

In the next part, the goal is to design the control inputs u_2 and u_3 such that i_{hfc} tracks the $i_{\text{ref}}(t)$. Let $v_3 = \ln(P_{\text{H}_2}) + (1/2)\ln(P_{\text{O}_2})$ to be the virtual control input in (2), $e_2 = i_{\text{hfc}} - i_{\text{ref}}$ and $e_3 = v_3 - v_{3\text{d}}$. Therefore,

$$
\dot{e}_2 = \frac{\text{d}i_{\text{hfc}}}{\text{d}t} - \dot{i}_{\text{ref}} = \frac{nR_{\text{g}}T_{\text{st}}}{2LF_{\text{ar}}}e_3 + \Gamma_1 + \frac{nR_{\text{g}}T_{\text{st}}}{2LF_{\text{ar}}}v_{3\text{d}} - \dot{i}_{\text{ref}}. \tag{12}
$$

Selecting $v_{3\text{d}} = ((2LF_{\text{ar}})/(nR_{\text{g}}T_{\text{st}}))(-\gamma_2 e_2 - \Gamma_1 + \dot{i}_{\text{ref}})$ provides

$$
\dot{e}_2 = \frac{nR_{\text{g}}T_{\text{st}}}{2LF_{\text{ar}}}e_3 - \gamma_2 e_2. \tag{13}
$$

Taking time derivative of the Lyapunov candidate $V_2 = (1/2)e_2^2$ along with the (13) results in

$$
\dot{V}_2 = e_2\dot{e}_2 = -\gamma_2 e_2^2 + \frac{nR_{\text{g}}T_{\text{st}}}{2LF_{\text{ar}}}e_2e_3. \tag{14}
$$

In the next stage, the dynamic of the error e_3 is computed as

$$
\begin{aligned}
\dot{e}_3 = \dot{v}_3 - \dot{v}_{3\text{d}} &= \frac{1}{P_{\text{H}_2}}\frac{\text{d}P_{\text{H}_2}}{\text{d}t} + \frac{1}{2P_{\text{O}_2}}\frac{\text{d}P_{\text{O}_2}}{\text{d}t} - \dot{v}_{3\text{d}}\\
&= -\frac{1}{\tau_{\text{H}_2}} + \frac{q_{\text{H}_2}^{\text{in}} - 2k_\gamma i_{\text{hfc}}}{\tau_{\text{H}_2}k_{\text{H}_2}P_{\text{H}_2}} - \frac{1}{2\tau_{\text{O}_2}} + \frac{q_{\text{O}_2}^{\text{in}} - 2k_\gamma i_{\text{hfc}}}{2\tau_{\text{O}_2}k_{\text{O}_2}P_{\text{O}_2}} - \dot{v}_{3\text{d}}\\
&= \Gamma_2 + \frac{q_{\text{H}_2}^{\text{in}}}{\tau_{\text{H}_2}k_{\text{H}_2}P_{\text{H}_2}} + \frac{q_{\text{O}_2}^{\text{in}}}{2\tau_{\text{O}_2}k_{\text{O}_2}P_{\text{O}_2}},
\end{aligned}
\tag{15}
$$

where $\Gamma_2 = -(1/\tau_{\text{H}_2}) - (1/(2\tau_{\text{O}_2})) - ((2k_\gamma i_{\text{hfc}})/(\tau_{\text{H}_2}k_{\text{H}_2}P_{\text{H}_2})) - ((k_\gamma i_{\text{hfc}})/(\tau_{\text{O}_2}k_{\text{O}_2})) - \dot{v}_{3\text{d}}$. Now, we define $e_4 = q_{\text{H}_2}^{\text{in}} - x_{4\text{d}}$ and $e_5 = q_{\text{O}_2}^{\text{in}} - x_{5\text{d}}$. Therefore,

$$
\dot{e}_3 = \frac{e_4}{\tau_{\text{H}_2}k_{\text{H}_2}P_{\text{H}_2}} + \frac{e_5}{2\tau_{\text{O}_2}k_{\text{O}_2}P_{\text{O}_2}} + \Gamma_2 + \frac{x_{4\text{d}}}{\tau_{\text{H}_2}k_{\text{H}_2}P_{\text{H}_2}} + \frac{x_{5\text{d}}}{2\tau_{\text{O}_2}k_{\text{O}_2}P_{\text{O}_2}}. \tag{16}
$$

Let us write

$$
\begin{aligned}
x_{4\text{d}} &= \tau_{\text{H}_2}k_{\text{H}_2}P_{\text{H}_2}\left(-\frac{\gamma_3}{2}e_3 - \frac{\Gamma_2}{2} - \frac{nR_{\text{g}}T_{\text{st}}}{4LF_{\text{ar}}}e_2\right),\\
x_{5\text{d}} &= 2\tau_{\text{O}_2}k_{\text{O}_2}P_{\text{O}_2}\left(-\frac{\gamma_3}{2}e_3 - \frac{\Gamma_2}{2} - \frac{nR_{\text{g}}T_{\text{st}}}{4LF_{\text{ar}}}e_2\right),
\end{aligned}
\tag{17}
$$

Therefore, (16) will be rewritten as follows:

$$
\dot{e}_3 = \frac{e_4}{\tau_{\text{H}_2}k_{\text{H}_2}P_{\text{H}_2}} + \frac{e_5}{2\tau_{\text{O}_2}k_{\text{O}_2}P_{\text{O}_2}} - \gamma_3 e_3 - \frac{nR_{\text{g}}T_{\text{st}}}{2LF_{\text{ar}}}e_2. \tag{18}
$$

Taking time derivative of $V_3 = V_2 + (1/2)e_3^2$ results in

$$
\begin{aligned}
\dot{V}_3 = \dot{V}_2 + e_3\dot{e}_3 &= -\gamma_2 e_2^2 + \frac{nR_{\text{g}}T_{\text{st}}}{2LF_{\text{ar}}}e_2e_3\\
&\quad + e_3\left(\frac{e_4}{\tau_{\text{H}_2}k_{\text{H}_2}P_{\text{H}_2}} + \frac{e_5}{2\tau_{\text{O}_2}k_{\text{O}_2}P_{\text{O}_2}} - \gamma_3 e_3 - \frac{nR_{\text{g}}T_{\text{st}}}{2LF_{\text{ar}}}e_2\right)\\
&= -\gamma_2 e_2^2 - \gamma_3 e_3^2 + \frac{e_3e_4}{\tau_{\text{H}_2}k_{\text{H}_2}P_{\text{H}_2}} + \frac{e_3e_5}{2\tau_{\text{O}_2}k_{\text{O}_2}P_{\text{O}_2}}.
\end{aligned}
\tag{19}
$$

In the final stage, we compute the dynamics e_4 and e_5 as follows:

$$
\dot{e}_4 = \dot{q}_{\text{H}_2}^{\text{in}} - \dot{x}_{4\text{d}} = \frac{u_2 - q_{\text{H}_2}^{\text{in}}}{\tau_{\text{qH}_2}} - \dot{x}_{4\text{d}}, \tag{20}
$$

$$
\dot{e}_5 = \dot{q}_{\text{O}_2}^{\text{in}} - \dot{x}_{5\text{d}} = \frac{u_3 - q_{\text{O}_2}^{\text{in}}}{\tau_{\text{qO}_2}} - \dot{x}_{5\text{d}}. \tag{21}
$$

Let the control inputs be

$$
u_2 = \tau_{\text{qH}_2}\left(-\gamma_4 e_4 - \frac{e_3}{\tau_{\text{H}_2}k_{\text{H}_2}P_{\text{H}_2}} + \frac{q_{\text{H}_2}^{\text{in}}}{\tau_{\text{qH}_2}} + \dot{x}_{4\text{d}}\right), \tag{22}
$$

$$
u_3 = \tau_{\text{qO}_2}\left(-\gamma_5 e_5 - \frac{e_3}{2\tau_{\text{O}_2}k_{\text{O}_2}P_{\text{O}_2}} + \frac{q_{\text{O}_2}^{\text{in}}}{\tau_{\text{qO}_2}} + \dot{x}_{5\text{d}}\right). \tag{23}
$$

Therefore, the dynamics (20) and (21) are simplified as follows:

$$
\begin{aligned}
\dot{e}_4 &= -\frac{e_3}{\tau_{\text{H}_2}k_{\text{H}_2}P_{\text{H}_2}} - \gamma_4 e_4,\\
\dot{e}_5 &= -\frac{e_3}{2\tau_{\text{O}_2}k_{\text{O}_2}P_{\text{O}_2}} - \gamma_5 e_5.
\end{aligned}
\tag{24}
$$

Taking time derivative of $V_4 = V_3 + (1/2)e_4^2 + (1/2)e_5^2$ results in

$$\dot{V}_4 = \dot{V}_3 + e_4\dot{e}_4 + e_5\dot{e}_5 - \gamma_2 e_2^2 - \gamma_3 e_3^2 + \frac{e_3 e_4}{\tau_{H_2} k_{H_2} P_{H_2}} + \frac{e_3 e_5}{2\tau_{O_2} k_{O_2} P_{O_2}} + e_4\left(-\frac{e_3}{\tau_{H_2} k_{H_2} P_{H_2}} - \gamma_4 e_4\right) + e_5\left(-\frac{e_3}{2\tau_{O_2} k_{O_2} P_{O_2}} - \gamma_5 e_5\right) = -\gamma_2 e_2^2 - \gamma_3 e_3^2 - \gamma_4 e_4^2 - \gamma_5 e_5^2. \quad (25)$$

Finally, by considering the Lyapunov candidate $V = V_4 + V_1$, we obtain

$$\dot{V} = -\gamma_1 e_1^2 - \gamma_2 e_2^2 - \gamma_3 e_3^2 - \gamma_4 e_4^2 - \gamma_5 e_5^2. \quad (26)$$

Since the time derivative of the Lyapunov function is negative definite, the error is asymptotically stable and the states V_{CPL} and i_{hfc} track the desired references. The proof is complete.

Remark 1 (difficulties of the design of the proposed controller). This work proposes a novel backstepping control law which is proposed for the marine power systems (1)–(7). These dynamics are not in the form of the conventional strict-feedback forms as the virtual inputs P_{H_2} and P_{O_2} are not affine in (2) and the overall dynamics comprise three control inputs. So, the conventional backstepping design procedure [32] is not applicable. However, in this paper, such difficulties are handled by (i) defining the tracking error e_3 as a nonlinear function of the virtual inputs, (ii) splitting the overall design procedure into two parts, and (iii) introducing an additional time-varying reference for the current of the fuel cell based on the properties of the nonlinear DC MG. These are the main distinctive features of the proposed approach over the existing backstepping techniques. The overall schematic of the proposed backstepping controllers to the regulate DC MG is given in Figure 3. Also, the detailed algorithm of deriving the control inputs u_1, u_2, and u_3 is given in Algorithm 1.

4. Model-in-the-Loop Results

In this section, to show the applicability and low computational time of the proposed nonlinear controller, we carry out a model-in-the-loop (MiL) real-time simulation [33]. For the MiL simulation as depicted in Figure 4, dSPACE 1202 board has been selected as the rapid prototyping solution. The solver is the Euler method, and the sampling frequency is 10 kHz. The MiL application of the suggested technique was done on a real-time simulator (RTS) wherein both the controller and grid system are embedded in a single RTS. The load-side converter tightly regulates the voltage of the ship engine. Therefore, the consuming power of the ship engine is constant and the overall converter and load act as a CPL. This control action is dependent on the proposed control actions u_1, u_2, and u_3. However, the load-side converter regulation action and the proposed control laws are designed by the dSPACE simulator.

First control input (u_1)
(1) Get V_{ref}.
(2) Compute $\dot{V}_{ref}$ and $e_1 = V_{CPL} - V_{ref}$.
(3) Compute ν_1 by (10).
(4) Apply the control input $u_1 = 1 - \nu_1$.
Second and third control inputs (u_2 and u_3)
(5) Get i_{ref}.
(6) Compute $\dot{I}_{ref}$ and $e_2 = i_{hfc} - i_{ref}$.
(7) Compute $\nu_{3d} = ((2LF_{ar})/(nR_gT_{st}))(-\gamma_2 e_2 - \Gamma_1 + \dot{i}_{ref})$.
(8) Compute $\dot{\nu}_{3d}$ and $e_3 = \nu_3 - \nu_{3d}$.
(9) Compute x_{4d} and x_{5d} by (17).
(10) Compute $\dot{x}_{4d}$, $\dot{x}_{5d}$, $e_4 = x_4 - x_{3d}$ and $e_5 = x_5 - x_{5d}$.
(11) Apply the control inputs (22) and (23).

Algorithm 1: The algorithm of computing control inputs.

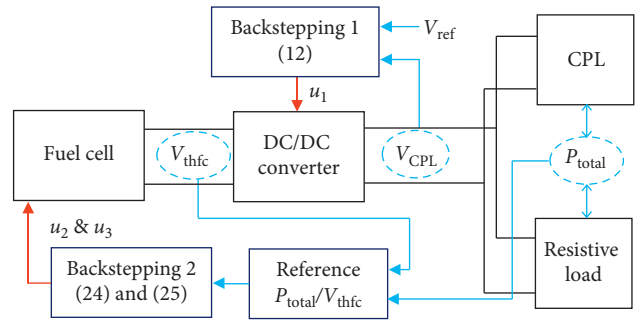

Figure 3: The overall schematic of the proposed control approach.

The MiL simulation is carried out for the system parameters given in Table 1 and the CPL voltage reference $V_{ref} = 400$ V. Note that, in practice, the parameters R_{at}, C_d, and R_{ohm} are uncertain parameters, but in the controller law, their nominal values given in Table 1 are considered.

Moreover, the control design parameters of the proposed backstepping controller are set as $\gamma_i = 1$ for $i = 1, 2, \ldots, 5$.

Furthermore, to show the performance improvement of the proposed approach, the sliding mode controller designed for the same case study in [10] is considered. In [10], in addition to the fuel cell, a supercapacitor is also connected to the DC bus through a buck/boost converter. Furthermore, only resistive loads are considered. However, to apply the sliding mode approach of [10] to the considered case study, the PWM input signal of the buck/boost converter is assumed to be zero and the dynamic of the DC bus voltage is updated to involve the CPL behavior. The parameters of the sliding mode controller and the way of its implementation are presented in [10].

Figures 5(a)–5(c) show the current, voltage, and generated power of the fuel cell, respectively, for both proposed approach and sliding mode controller [10].

As one can see in Figures 5(a)–5(c), the proposed approach leads to a more smooth current and voltage for the fuel cell and less power fluctuation than in [10]. The main source of these fluctuations is uncertainties in the fuel cell

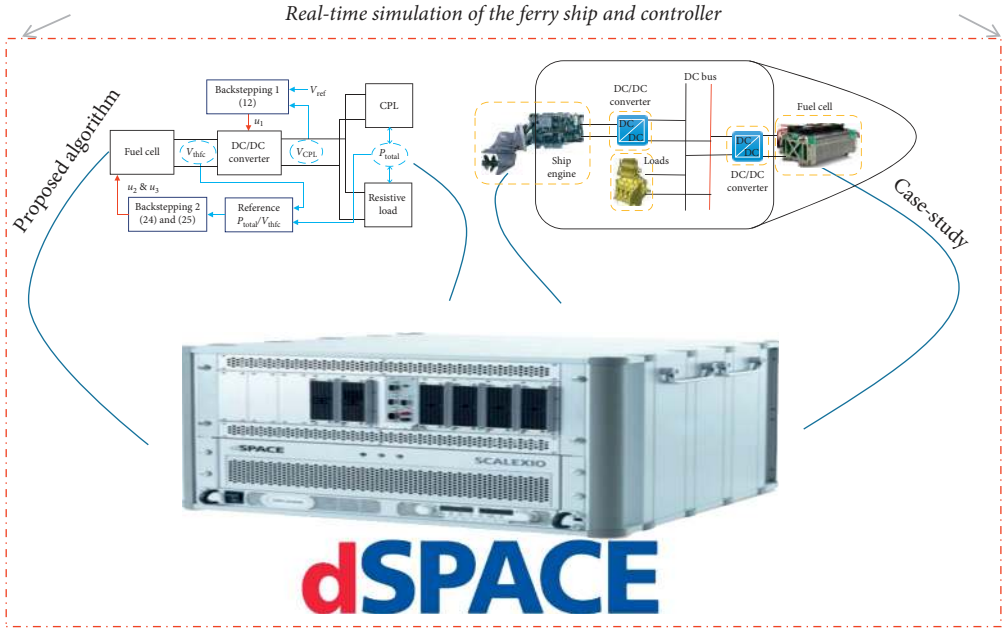

(a)

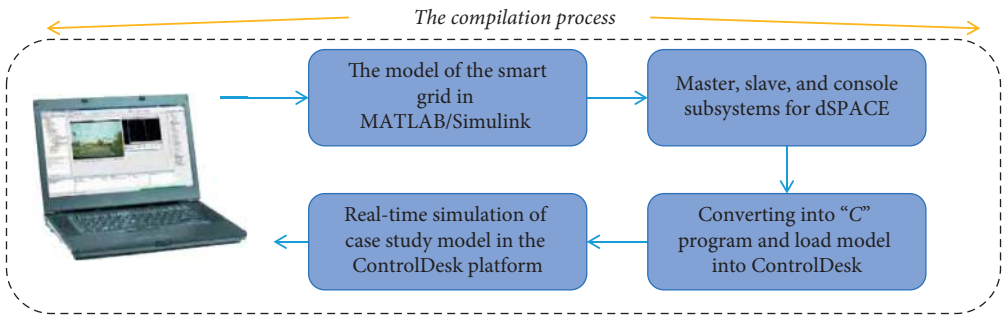

(b)

Figure 4: MiL real-time setup and configuration of the marine DC MG benchmark.

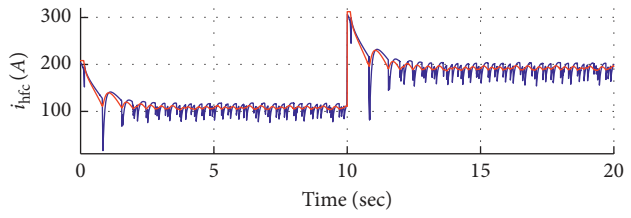

(a)

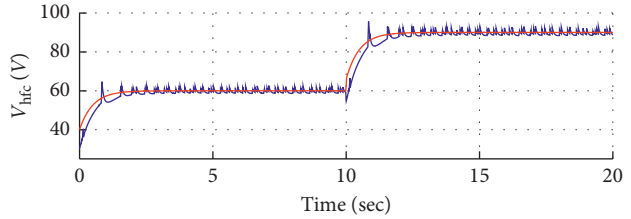

(b)

Figure 5: Continued.

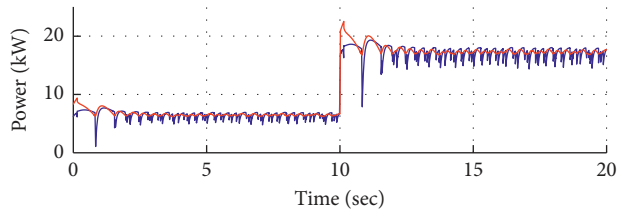

(c)

Figure 5: The (a) current, (b) voltage, and (c) generated power of the fuel cell (the proposed approach by the red line and the sliding mode approach by the blue line).

parameters. Since both the proposed sliding mode approaches use the nominal values and the considered fuel cell dynamics are severely nonlinear, power and voltage fluctuations are inevitable.

Figure 6 illustrates the voltage of the DC bus for both approaches. Figure 6 reveals reliable marine DC MG. The reason is that the voltage of the DC bus (i.e., the CPL voltage) is regulated to its desired reference better and more accurate than that of [10]. For instance, the DC bus voltage based on the proposed controller converges to its reference almost at $t = 2$ sec and the fluctuation amplitude is less than 2V. However, the sliding mode approach [10] leads to about 6V fluctuations in the DC bus voltage.

However, from Figure 7, one concludes that there are still some oscillations in the DC but voltage, especially, when the power level of the CPL changes promptly at $t = 10$ sec. The reason is that the fuel cell generator is a slow-response unit and it takes time to precisely regulate its power. Since there are no other fast-response units such as a battery or a supercapacitor, the injecting power to the CPL and resistive load is not constant and equal to the demand power. So, the resistive load receives nonconstant power and its voltage is changed by time.

The power received to the resistive load is illustrated in Figure 7. As can be seen in Figures 5(c) and 7, the proposed approach provides a smoother power than the sliding mode approach [10]. Furthermore, the approach of [10] injects more extra power to the resistive load. The ideal value for the resistive load power is 2kW, for which the DC but voltage will kept at 400V. The higher injected power not only reduces the performance of the system but also results in more hydrogen and oxygen consumption. Therefore, the compressed tanks for the hydrogen and oxygen will be emptied faster than the proposed approach. However, note that the power surplus (undersupply) and the voltage oscillation can be compensated by connecting a battery or a supercapacitor to the DC bus. However, in this paper, such compensation is not considered and only the attempt was made to propose a novel nonlinear control approach to enhance the transient and steady-state regulation of the hydrogen fuel cell.

Moreover, to show the steady-state performance of the proposed approach and the sliding mode control [10], Table 2 is provided. As can be seen in Table 2, the steady-state error of the proposed approach is more than 60 % which is improved over the sliding mode approach [10].

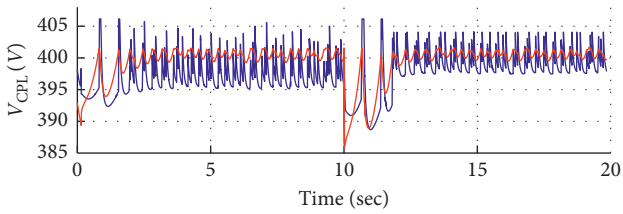

Figure 6: The voltage of the DC bus (the proposed approach by the red line and the sliding mode approach by the blue line).

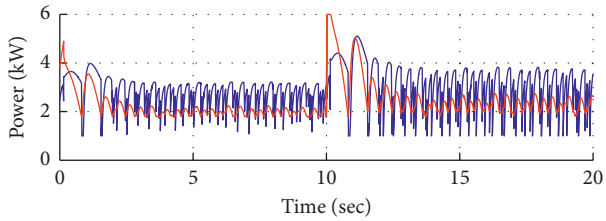

Figure 7: The injected power to the resistive load (the proposed approach by the red line and the sliding mode approach by the blue line).

Table 2: Steady-state error of different approaches.

	Proposed approach	Sliding mode approach [10]	Performance improvement (%)
V_{CPL}	1.572	4.103	61.68
i_{hfc}	3.637	47.323	92.31
V_{hfc}	0	3.191	100
Power	498.344	1578.723	68.43 %

5. Conclusion

The goal of this research was to stabilize a special DC marine MG that has uncertain time-varying loads and drive the DC voltage of the bus to track the desired voltage. To this aim, an additional reference for the current of the hydrogen fuel cell is defined and the controller design procedure is carried out by considering two backstepping controllers operating in parallel. To implement the controllers, first, some nonlinear error dynamics are defined to facilitate stabilizing the non-strict-feedback model of the system. Then, the virtual control signals are obtained step by step, by constructing suitable control Lyapunov functions (CLF) and providing the stability conditions, until the desired control signal is obtained. To illustrate

the effectiveness of the proposed controller, it is compared with the state-of-the-art method sliding mode controller. The real-time simulation results demonstrated the ability of the proposed controller in tracking the desired voltage of the bus for sudden and continuous changes of the load power.

Data Availability

The data used to support the findings of this study are available from the corresponding author upon request.

Conflicts of Interest

The authors declare that there are no conflicts of interest regarding the publication of this paper.

Acknowledgments

This work was supported by the Energy Technology Development and Demonstration Program (EUDP) under Grant (64018-0721), "HFC: Hydrogen Fuel Cell and Battery Hybrid Technology for Marine Applications".

References

[1] J. Han, J.-F. Charpentier, and T. Tang, "An energy management system of a fuel cell/battery hybrid boat," *Energies*, vol. 7, no. 5, pp. 2799–2820, 2014.

[2] M.-H. Khooban, T. Dragicevic, F. Blaabjerg, and M. Delimar, "Shipboard microgrids: a novel approach to load frequency control," *IEEE Transactions on Sustainable Energy*, vol. 9, no. 2, pp. 843–852, 2018.

[3] M. H. Khooban and M. Gheisarnejad, "Islanded microgrid frequency regulations concerning the integration of tidal power units: real-time implementation," *IEEE Transactions on Circuits and Systems II: Express Briefs*, pp. 1–11, 2019.

[4] M. Gheisarnejad, M.-H. Khooban, and T. Dragicevic, "The future 5G network based secondary load frequency control in maritime microgrids," *IEEE Journal of Emerging and Selected Topics in Power Electronics*, p. 1, 2019.

[5] A. Miola, B. Ciuffo, E. Giovine, and M. Marra, "Regulating air emissions from ships: the state of the art on methodologies, technologies and policy options," Reference reports, Publications Office of the European Union, Brussels, Belgium, 2010.

[6] L. K. C. Tse, S. Wilkins, N. McGlashan, B. Urban, and R. Martinez-Botas, "Solid oxide fuel cell/gas turbine trigeneration system for marine applications," *Journal of Power Sources*, vol. 196, no. 6, pp. 3149–3162, 2011.

[7] J. T. Pukrushpan, H. Peng, and A. G. Stefanopoulou, "Control-oriented modeling and analysis for automotive fuel cell systems," *Journal of Dynamic Systems, Measurement, and Control*, vol. 126, no. 1, p. 14, 2004.

[8] M. Gheisarnejad, J. Boudjadar, and M.-H. Khooban, "A new adaptive type-II fuzzy-based deep reinforcement learning control: fuel cell air-feed sensors control," *IEEE Sensors Journal*, vol. 19, no. 20, pp. 9081–9089, 2019.

[9] S. Bahrebar, F. Blaabjerg, H. Wang et al., "A novel type-2 fuzzy logic for improved risk analysis of proton exchange membrane fuel cells in marine power systems application," *Energies*, vol. 11, p. 721, 2018.

[10] R. Ashok and Y. Shtessel, "Control of fuel cell-based electric power system using adaptive sliding mode control and observation techniques," *Journal of the Franklin Institute*, vol. 352, no. 11, pp. 4911–4934, 2015.

[11] F. Li, Y. Yuan, X. Yan, R. Malekian, and Z. Li, "A study on a numerical simulation of the leakage and diffusion of hydrogen in a fuel cell ship," *Renewable and Sustainable Energy Reviews*, vol. 97, pp. 177–185, 2018.

[12] L. van Biert, M. Godjevac, K. Visser, and P. V. Aravind, "A review of fuel cell systems for maritime applications," *Journal of Power Sources*, vol. 327, pp. 345–364, 2016.

[13] P. Thounthong, S. Rael, and B. Davat, "Control strategy of fuel cell and supercapacitors association for a distributed generation system," *IEEE Transactions on Industrial Electronics*, vol. 54, no. 6, pp. 3225–3233, 2007.

[14] S. Vazquez, J. Rodriguez, M. Rivera, L. G. Franquelo, and M. Norambuena, "Model predictive control for power converters and drives: advances and trends," *IEEE Transactions on Industrial Electronics*, vol. 64, no. 2, pp. 935–947, 2017.

[15] C. Damour, M. Benne, C. Lebreton, J. Deseure, and B. Grondin-Perez, "Real-time implementation of a neural model-based self-tuning PID strategy for oxygen stoichiometry control in PEM fuel cell," *International Journal of Hydrogen Energy*, vol. 39, no. 24, pp. 12819–12825, 2014.

[16] S. M. Rakhtala, A. R. Noei, R. Ghaderi, and E. Usai, "Design of finite-time high-order sliding mode state observer: a practical insight to PEM fuel cell system," *Journal of Process Control*, vol. 24, no. 1, pp. 203–224, 2014.

[17] N. Vafamand, M. H. Khooban, T. Dragicevic, and F. Blaabjerg, "Networked fuzzy predictive control of power buffers for dynamic stabilization of DC microgrids," *IEEE Transactions on Industrial Electronics*, vol. 66, no. 2, pp. 1356–1362, 2019.

[18] L. Ding, Q.-L. Han, L. Y. Wang, and E. Sindi, "Distributed cooperative optimal control of DC microgrids with communication delays," *IEEE Transactions on Industrial Informatics*, vol. 14, no. 9, pp. 3924–3935, 2018.

[19] M. A. Kardan, M. H. Asemani, A. Khayatian et al., "Improved stabilization of nonlinear DC microgrids: cubature Kalman filter approach," *IEEE Transactions on Industry Applications*, vol. 54, no. 5, pp. 5104–5112, 2018.

[20] N. Vafamand, M. H. Khooban, T. Dragicevic, F. Blaabjerg, and J. Boudjadar, "Robust non-fragile fuzzy control of uncertain DC microgrids feeding constant power loads," *IEEE Transactions on Power Electronics*, vol. 34, 2019.

[21] E. Hossain, "Addressing instability issues in microgrids caused by constant power loads using energy storage systems," Theses and Dissertations, University of Wisconsin-Milwaukee, Milwaukee, WI, USA, 2016.

[22] N. Vafamand, A. Khayatian, and M. H. Khooban, "Stabilisation and transient performance improvement of DC MGs with CPLs: non-linear reset control approach," *IET Generation, Transmission & Distribution*, vol. 13, no. 14, pp. 3169–3176, 2019.

[23] J. Wu and Y. Lu, "Adaptive backstepping sliding mode control for boost converter with constant power load," *IEEE Access*, vol. 7, pp. 50797–50807, 2019.

[24] N. Vafamand, S. Yousefizadeh, M. H. Khooban, J. D. Bendtsen, and T. Dragicevic, "Adaptive TS fuzzy-based MPC for DC microgrids with dynamic CPLs: nonlinear power observer approach," *IEEE Systems Journal*, vol. 13, pp. 1–8, 2018.

[25] H. Farsizadeh, M. Gheisarnejad, M. Mosayebi, M. Rafiei, and M. H. Khooban, "An intelligent and fast controller for DC/DC converter feeding CPL in a DC microgrid," *IEEE Transactions On Circuits And Systems II: Express Briefs*, p. 1, 2019.

[26] T. Dragicevic, "Dynamic stabilization of DC microgrids with predictive control of point of load converters," *IEEE Transactions on Power Electronics*, vol. 33, p. 1, 2018.
[27] R. Cheng, J. F. Forbes, and W. S. Yip, "Price-driven coordination method for solving plant-wide MPC problems," *Journal of Process Control*, vol. 17, no. 5, pp. 429–438, 2007.
[28] Y. Zhao, W. Qiao, and D. Ha, "A sliding-mode duty-ratio controller for DC/DC buck converters with constant power loads," *IEEE Transactions on Industry Applications*, vol. 50, no. 2, pp. 1448–1458, 2014.
[29] A. M. Rahimi and A. Emadi, "Active damping in DC/DC power electronic converters: a novel method to overcome the problems of constant power loads," *IEEE Transactions on Industrial Electronics*, vol. 56, no. 5, pp. 1428–1439, 2009.
[30] J. T. Pukrushpan, A. G. Stefanopoulou, and H. Peng, *Control of Fuel Cell Power Systems*, Springer London, London, UK, 2004.
[31] W. K. Na and B. Gou, "Feedback-linearization-based nonlinear control for PEM fuel cells," *IEEE Transactions on Energy Conversion*, vol. 23, no. 1, pp. 179–190, 2008.
[32] S. Yousefizadeh, J. D. Bendtsen, N. Vafamand, M. H. Khooban, T. Dragicevic, and F. Blaabjerg, "Tracking control for a DC microgrid feeding uncertain loads in more electric aircraft: adaptive backstepping approach," *IEEE Transactions on Industrial Electronics*, vol. 66, no. 7, pp. 5644–5652, 2018.
[33] M. Gheisarnejad, P. Karimaghaee, J. Boudjadar, and M.-H. Khooban, "Real-time cellular wireless sensor testbed for frequency regulation in smart grids," *IEEE Sensors Journal*, pp. 1–11, 2019.